Supplemental Information

Supplemental Figure Legends

Figure S1. Phospho-mimetic CENP-T, but not phospho-deficient CENP-T, directly binds to the Spc24/25 portion of the Ndc80 complex.

(A) Stoichiometric amount of CENP-T(2-98 aa) D mutant (T16D, S24D, T56D, T72D, and S88D) fused with MBP (MBP-CENP-T^{2-98})and globular domain of the Spc24/25 complex were mixed and incubated for 15 min at room temperature. The mixture was separated by gel filtration using a Superdex 75. Peak fractions were analyzed by SDS-PAGE.

(B) CG-MALS analysis of phospho-mimetic chicken MBP-CENP-T^{2-98} together with the globular domain of the chicken $Spc24^{125-195}$/$Spc25^{132-234}$ complex. Two components interacted with 1:1 stoichiometry and the Kd was 480nM.

(C) Gel filtration experiment as in (A) of MBP-CENP-T^{63-98} T72A and S88A with the chicken $Spc24^{125-195}$/$Spc25^{132-234}$ complex.

(D) Coomassie-stained gels of fractions from a gel filtration assessing the co-migration of stoichiometric amounts of chicken MBP-CENP-T^{2-50} T16D and S24D with the globular domains of the chicken Spc24/25 complex (as in (A)).

(E) Coomassie-stained gels of fractions from a gel filtration assessing the co-migration of stoichiometric amounts of unphosphorylated human MBP-CENP-T^{76-106} with the globular domain of the human $Spc24^{131-197}$/$Spc25^{129-224}$ complex.

(F) Coomassie-stained gels of fractions from a gel filtration assessing the co-migration of stoichiometric amounts of MBP-hsCENP-T^{76-106} (T85D) with the globular domain of the human $Spc24^{131-197}$/$Spc25^{129-224}$ complex.

(G) ITC binding curve for the interaction of unphosphorylated MBP-hsCENP-T^{76-106} with the globular domain of the human $Spc24^{131-197}$/$Spc25^{129-224}$ complex. Kd is 645 nM.

(H) ITC binding curve for the interaction of MBP-hsCENP-T^{76-106} (T85D) with the globular domain of the human $Spc24^{131-197}$/$Spc25^{129-224}$ complex. Kd is 150 nM.

Figure S2. The human CENP-T N-terminal region binds to the $Ndc80^{Bonsai}$ complex, but not to the Mis12 complex.

(A) The MBP-fused unphosphorylated or phosphomimetic (T85D) human CENP-T^{76-106}

and the Ndc80^{Bonsai} complex were mixed and analyzed by gel filtration chromatography.

(B) The human unphosphorylated CENP-T N-terminal region (1-375 aa) or the human phosphomimetic CENP-T N-terminal region (T85D) and the Ndc80^{Bonsai} complex were mixed and analyzed by gel filtration chromatography.

(C) The human phospho-mimetic CENP-T N-terminal region (1-375 aa, T85D) and the Mis12 complex were mixed and analyzed by gel filtration chromatography.

Figure S3. Sequence comparison of CENP-T N-terminus in various species.

(A) Sequence alignment of CENP-T from various species. The conserved T-P-R motif is highlighted. The motif is diverged in some species. Phylogenetic tree is also shown.

(B) Prediction of the unstructured region of CENP-T from chicken, human, *S. pombe*, and *N. crassa* by the DISOPRED2 prediction tool. Disordered-probability is shown as green. Prediction of α-helical regions is shown in red. Potential CDK sites are also shown. The blue shading indicates the Spc24/25 complex binding region. The shaded yellow region in *S. pombe*, and *N. crassa* is predicted as the Spc24/25 binding region based on sequence comparison and helix probabilities.

Figure S4. Binding region of Spc24 and 25 to CENP-T in various species.

Sequence alignment of Spc24 and Spc25 from chicken, human, mouse, fission yeast, and budding yeast. Residues involved in interactions with CENP-T are denoted by magenta. Secondary structures are also indicated.

Figure S5. Binding of CENP-T and the Mis12 complex to Spc24/25 is mutually exclusive.

(A) I149A_L154A double mutants in human Spc25 disrupt binding to human CENP-T. Human phospho-mimetic CENP-T (MBP-hsCENP-T$^{76-106}$T85D) and the wild-type Spc24$^{57-197}$/Spc25$^{70-224}$ complex or the Spc24$^{57-197}$/Spc25$^{70-224}$ complex (I149A L154A for Spc25) mutant complex were mixed and analyzed by gel filtration using a Superdex 200 column. Fractions were collected, analyzed by SDS-PAGE, and stained with Coomassie.

(B) ITC binding curve for the interaction of the human wild-type Spc24$^{57-197}$/Spc25$^{70-224}$ complex or the Spc24$^{57-197}$/Spc25$^{70-224}$ complex (I149A L154A for Spc25) mutant

complex with human phospho-mimetic CENP-T (MBP-hsCENP-T$^{76\text{-}106}$T85D). The measured K_D's for interaction of the wild-type Spc24$^{57\text{-}197}$/Spc25$^{70\text{-}224}$ complex and the mutant Spc24/25 complex with human CENP-T are 58.1 nM and 94 μM, respectively.

(C) The wild-type the Spc24$^{57\text{-}197}$/Spc25$^{70\text{-}224}$ complex or the Spc24$^{57\text{-}197}$/Spc25$^{70\text{-}224}$ complex (I149A L154A for Spc25) mutant complex and the human Mis12-KNL1$^{2106–2316}$ complex were mixed and analyzed by gel filtration chromatography using a Superdex 200 column. Fractions were collected, analyzed by SDS-PAGE, and stained with Coomassie.

(D) ITC binding curve for the interaction of the human Spc24$^{57\text{-}197}$/Spc25$^{70\text{-}224}$ complex (wild-type or I149A L154A double mutants) with the Mis12/KNL1^{CT} complex. The measured K_D's for interaction of the wild-typeSpc24$^{57\text{-}197}$/Spc25$^{70\text{-}224}$ complex and the mutant Spc24/25 complex with human Mis12/KNL1^{CT} complex are 18.9 nM and 291 nM, respectively.

(E) CENP-T and the Mis12/KNL1^{CT} complex show mutually exclusive binding to the Spc24/25 complex. Human phospho-mimetic CENP-T, the human wild-type Spc24$^{57\text{-}197}$/Spc25$^{70\text{-}224}$ complex, and the human Mis12-KNL1$^{2106–2316}$ complex were mixed and analyzed by gel filtration. Fractions were collected, analyzed by SDS-PAGE, and stained with Coomassie. A large complex containing all components was not detected, although both CENP-T and KNL1/Mis12 bound individually to the Spc24/25 complex based on altered migration.

Figure S6. Creation of Spc25-conditinal knock-out, Dsn1-degron, and CENP-T-degron cells.

(A) Restriction maps of the chicken Spc25 locus, the gene disruption constructs, and the targeted locus. Black boxes indicate the positions of exons, and the targeted constructs that are expected to disrupt the entire region of the gene. XbaI and XhoI restriction sites are shown. The position of the probe used for Southern hybridization is indicated. Novel 9.4 kb or 7.5 kb fragments digested with XbaI will hybridize to the probe if the targeted integrations of the constructs occur.

(B) Restriction analysis of the targeted integration of the Spc25 disruption constructs. Genomic DNA from wild-type DT40 cells, a clone after the first round targeting (+/-, 1st) and a clone after the second round targeting (-/- Spc25 cDNA+) were

digested with XbaI and analyzed by Southern hybridization with the probe indicated in (A). Expression of Spc25 cDNA is repressed by addition of tet in the clone after the second round targeting.

(C) Ndc80 localization is eliminated Spc25-conditinal knock-out cells. Immuofluorescence images of cells 24 h after the addition of tet to Spc25 OFF cells. Bar, 10 μm.

(D) Immunofluorescence analysis of Ndc80 in Dsn1- or CENP-T-degron cells. Endogenous Dsn1 or CENP-T was replaced with auxin-degron tagged Dsn1 or CENP-T, respectively. Cells were synchronized at mitosis and Dsn1 and CENP-T were degraded by addition of auxin (IAA). Degron tagged proteins were undetected in 1 h after addition of IAA. Ndc80 signals are reduced ~43% and ~32% in CENP-T- and DsnI-degron cells, respectively. Ndc80 signal intensities were measured relative to an adjacent background signal. Bar, 10 μm.

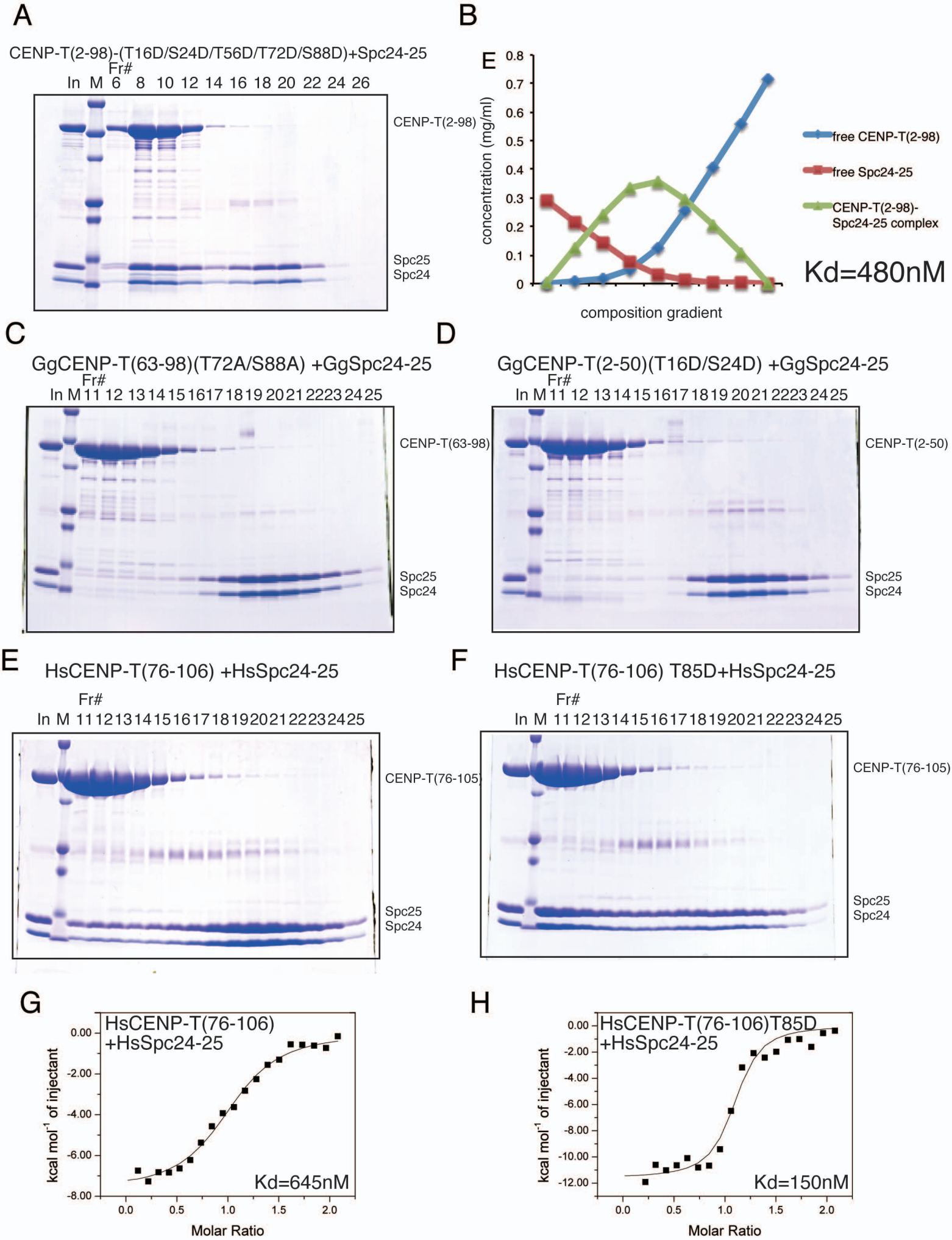

Nishino et al., 2012 Figure S1

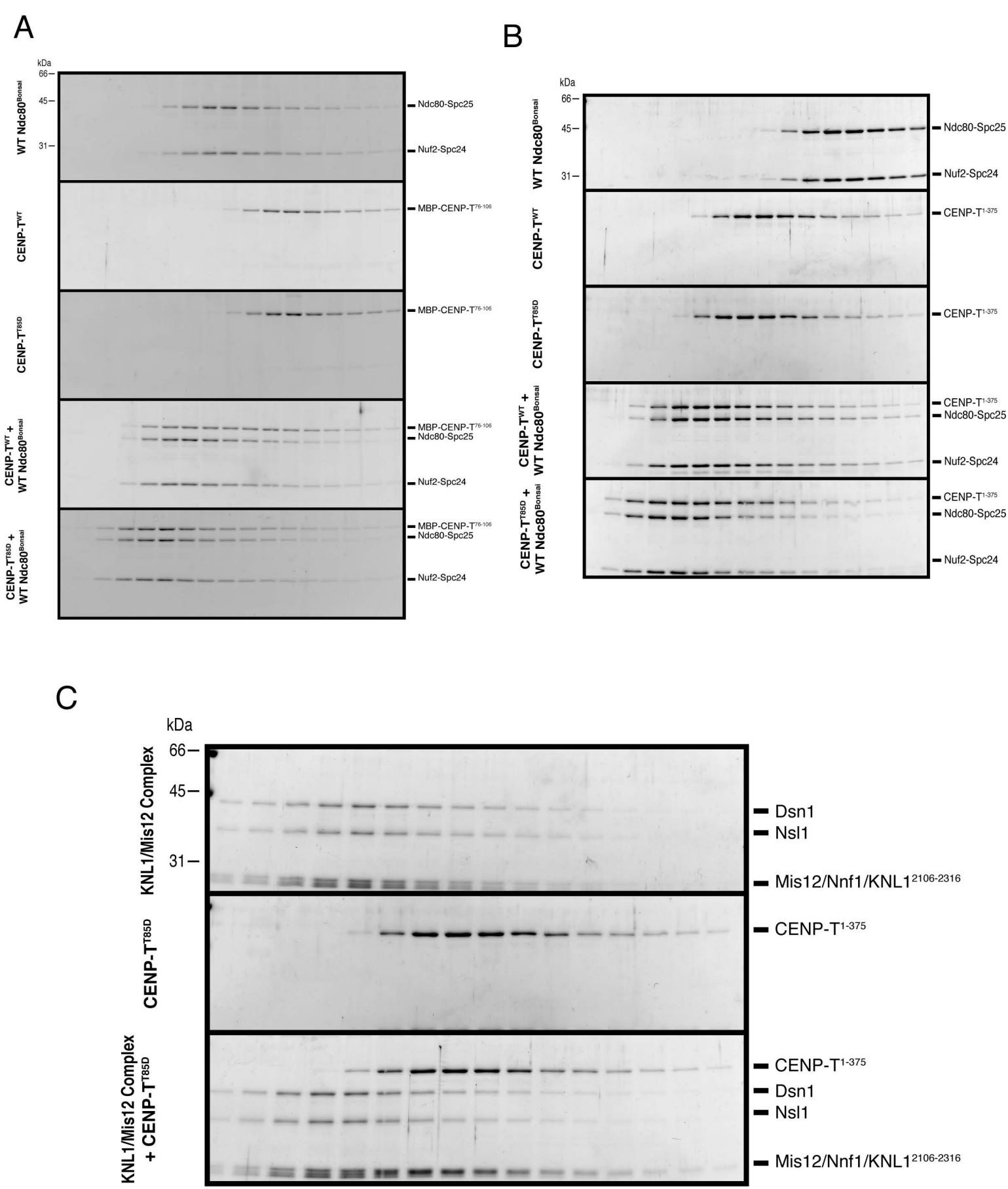

Nishino et al., 2012 Figure S2

A

```
Saccharomyces cer.   KDPNEVRSFLQDLSQVLARKSQGNDTTTNKTQA
Zygosaccharomyc      KDPSEVKEYLRDLSSVLVSQGRNLTSFLAEQVS
Ashbya               RDPQKLRHYLRELSSVLVNVSESPVPSSAQAEP
Saccharomyces klu.   KDPLELSTYLRELSTVLLEQKDRDEQFHESRKQ
Chaetomium           EVRDSPRDFLLSLGRVLARTTEVITTSSSPS--
Myceliophthora       EVRDSPRDFLLSLGRVLARNTEVITTSSSSSPG
Thielavia            EVRDSPRDFLLSLGRVLARTTQVITTSSSSS-S
Podospora            EARDSPRDLLLGLGRVLAKKTEPIVTSSSSPGD
Chaetomium           ETRDSPRDFLLSLAGVLATKSQRVVTSSSSSAR
Sordaria             EARETPRNFLLQLGKVLAPKSERIPSSSSSP-G
Neurospora           EARETPRNFLLQLGKVLAPKSERIPSSSSSP-A
Nectria              QQRETPLDILRTLGRVLAPTSKPIQTSSSSSPD
Fusarium             QQRETPLDILRMLGRTLAPKSQPIHSSSSSSPG
Gibberella           QQRETPLDVLRHLGRALAPKSKPIQYSSSSSPG
Neosartorya          IQRETTFDILRNLGKALAPISQPIRSSPQEKLE
Aspergillus          IERETTFDILRNLGKALAPVSQPIQSSPQERLE
Arthroderma          FKRETPMDILKNLGKALAPISKPVSSSPQTELE
Trichophyton         FKRETPMDILKNLGKVLAPVSKTVSSSPPAESE
Penicillium          PQQETAFDILRNLGRTLAPISKPIQSSPQEERS
Talaromyces          PQRETAFDILRNLGRTLAPISKPIQSSPQDERS
Ajellomyces          MQRETPMDVLRNLGKVLAPTTRPVSSSPQEEPE
Paracoccidioides     VQRETPMDILRNLGKVLAPNTRTVSSSPTEKPE
Coccidioides         VQRETPLDILRNLGKALAPTSEVIKSSPMTETD
Botryotinia          QQRETPRDVLRLLSRTLAPQTRPTIPSPQRAPS
Leptosphaeria        MQRETPRDLLRGLSRALARDSRPVQPSPQVQAK
Pyrenophora          IQRETPRDILRDLARALARDSRPIEPSPQLPPP
Grosmannia           YLRESPRDLLRNLSRRLAPISQPVATSSSPAFS
Schizosaccharomyces  FSATTPRDILRMLSRALAKNPVP---SPAESES
Tuber                AARETPRDLLRALSRQLATTSTQYVPSPAQPAP
Verticillium         RRRESLFDNLRALSQALAPRSKPVETSSSPRDV
Glomerella           PRRESIHDILRGLSRVVKHDTQPISSSSSPSDL
Cordyceps            EQHQTPMNILNQLARRLAPSTQQVAASSSPAER
Magnaporthe          PQKDGPFDALRHLSRRLAPQTERVVTSSSPGDV
Xenopus              LDGITPRSLLRKIIQN-EPEVSLIVSQKYDPVA
Gallus               LDSATPRVMLRRIIQN-QPQVSPLALQTVQLEE
Homo                 LEEQTPRTLLKNILLT-APESSILMPESVVKPV
Mus                  LEEQTPRTLLRNILLT-APESSTVMPDPVVKPA
Dicentrarchus        DDGDTPRHILMNILRT-EPVRSPVVHEKAASEE
```

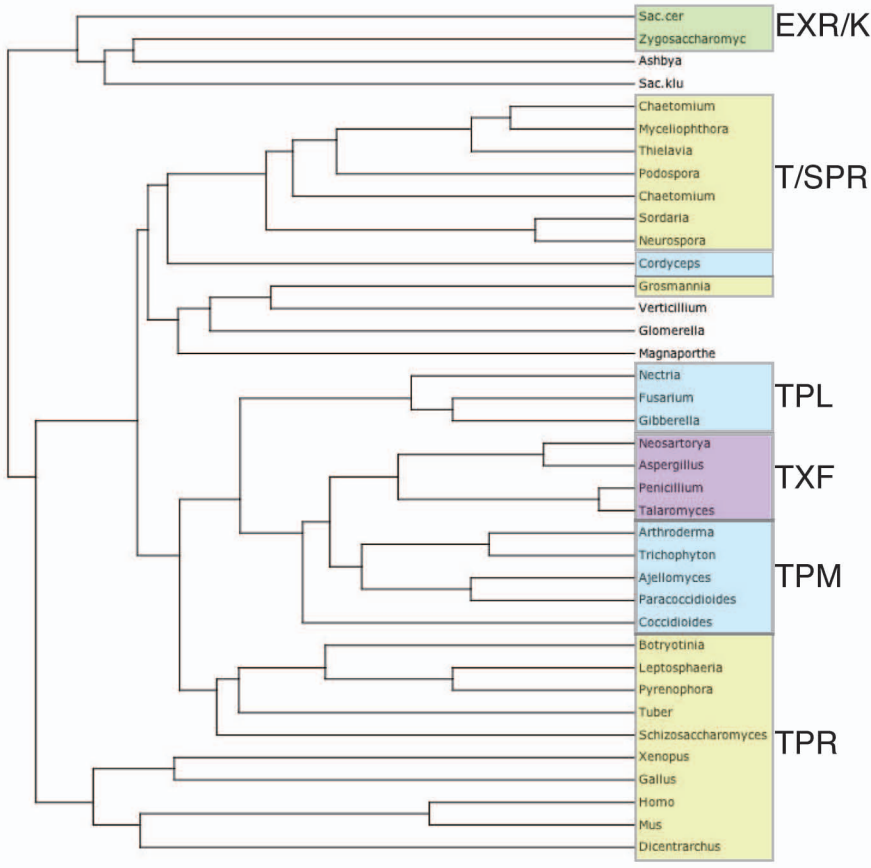

B

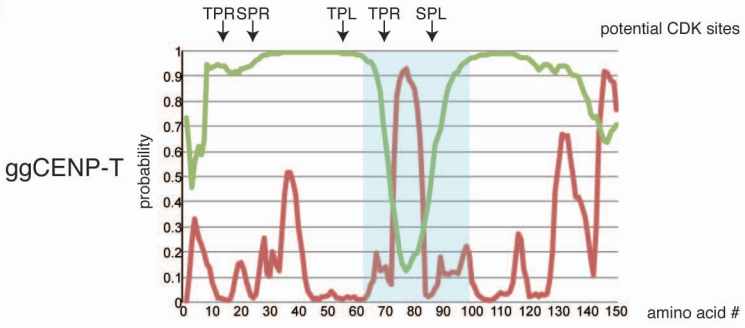

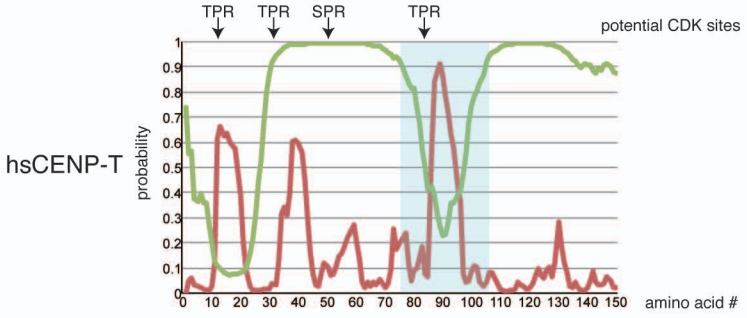

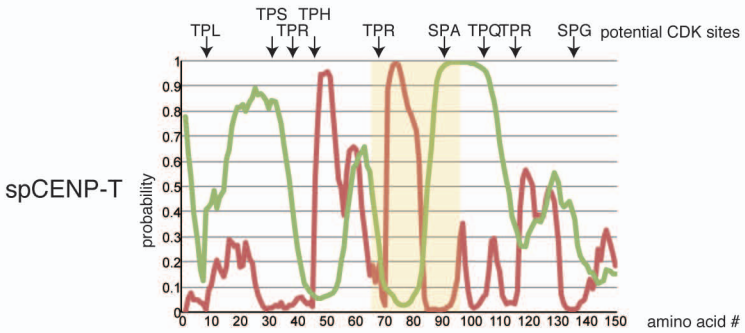

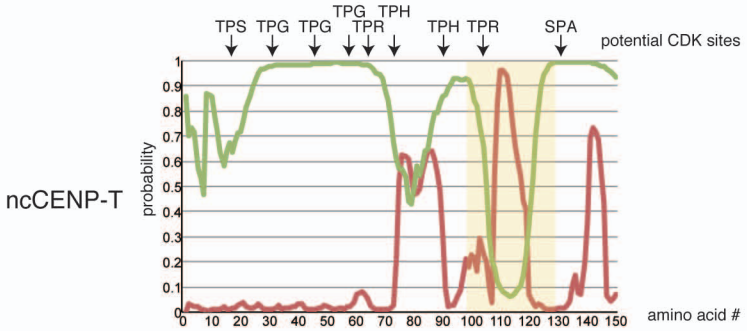

Nishino et al., 2012 Figure S3

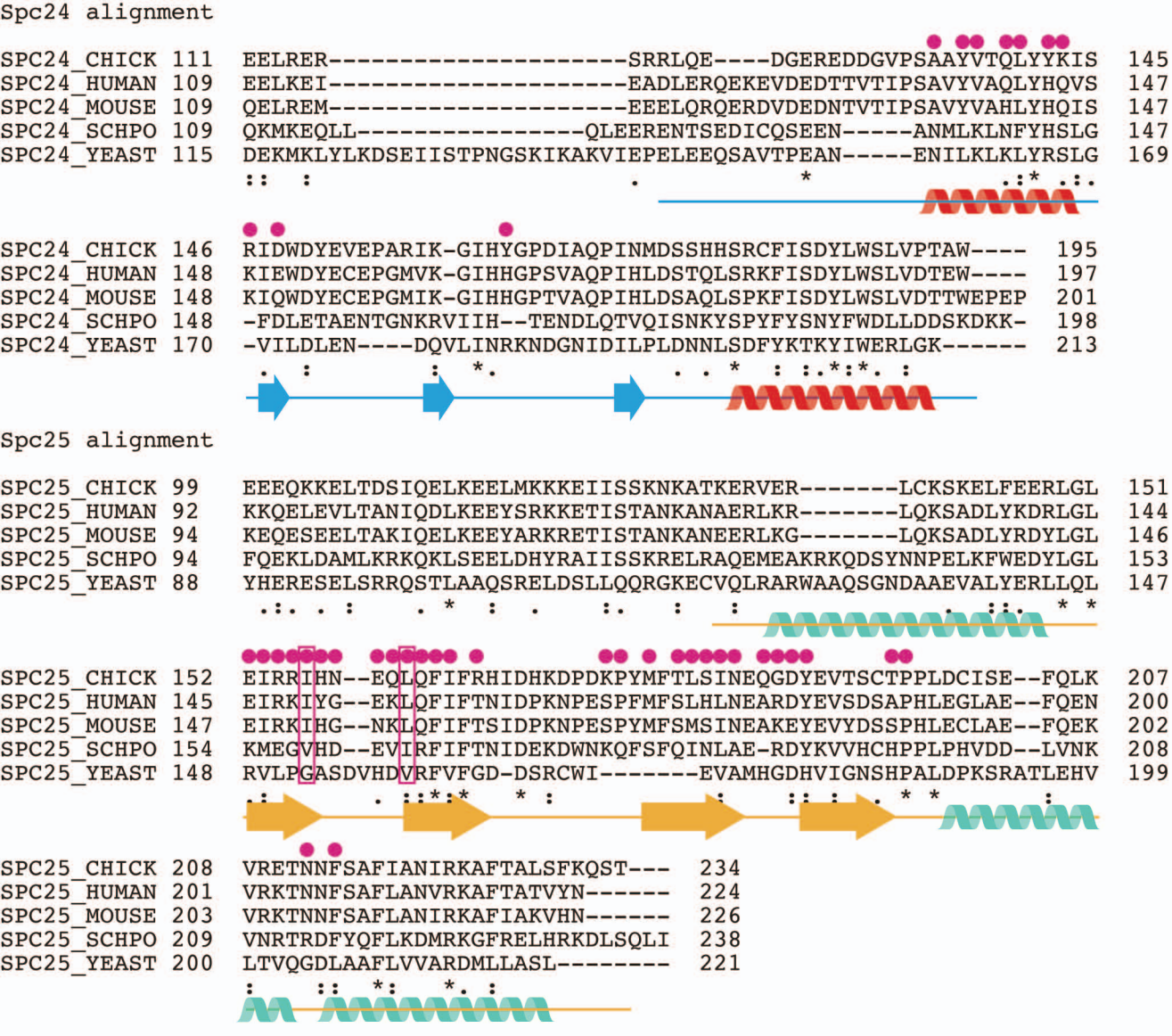

Nishino et al., 2012 Figure S4

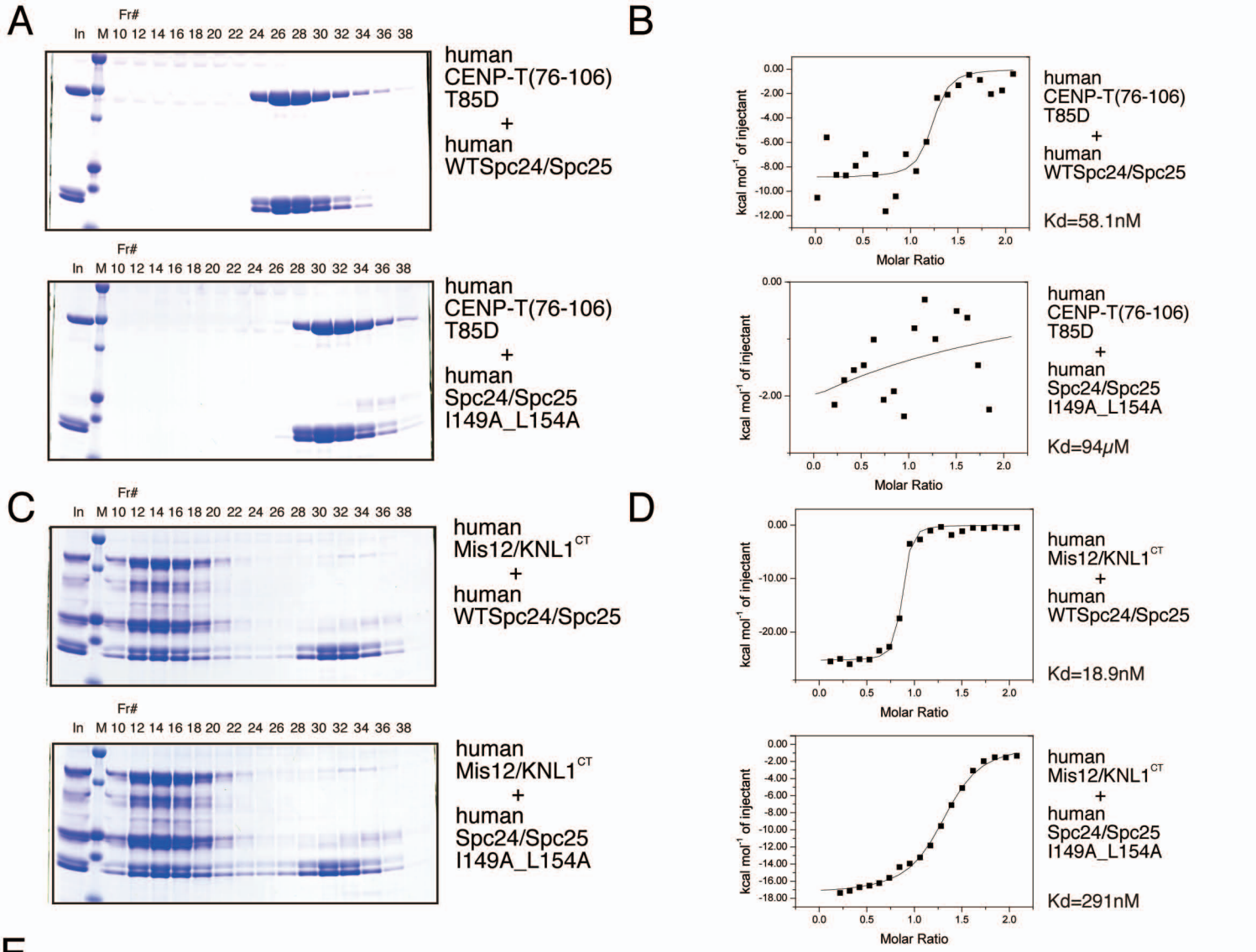

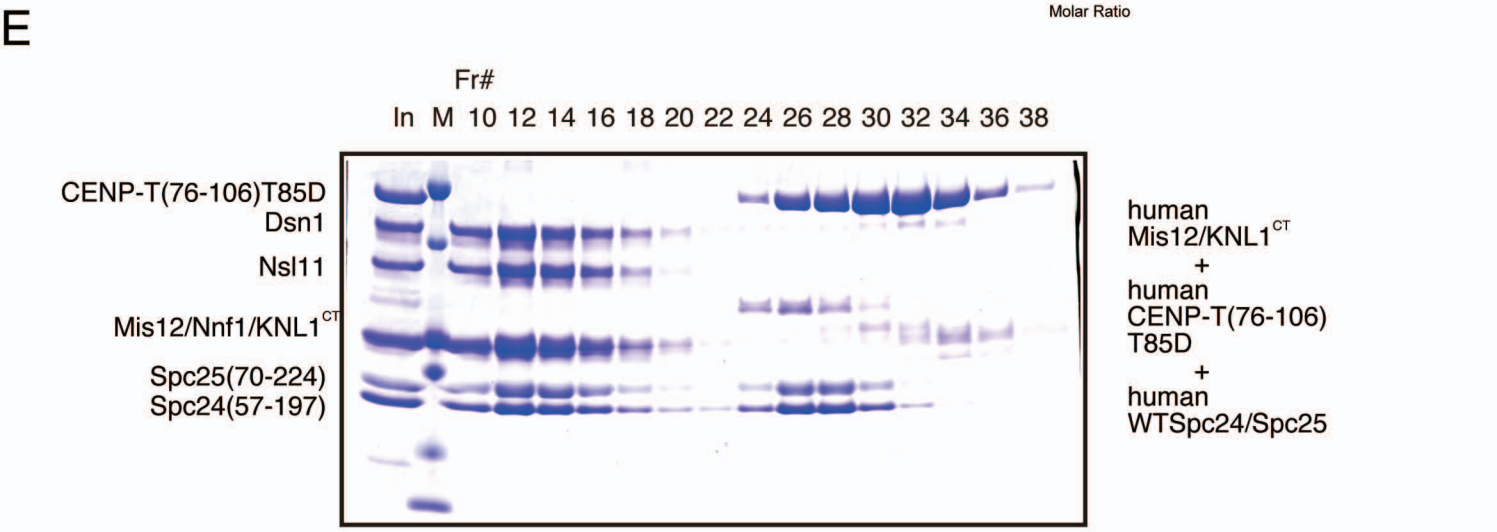

Nishino et al., 2012 Figure S5

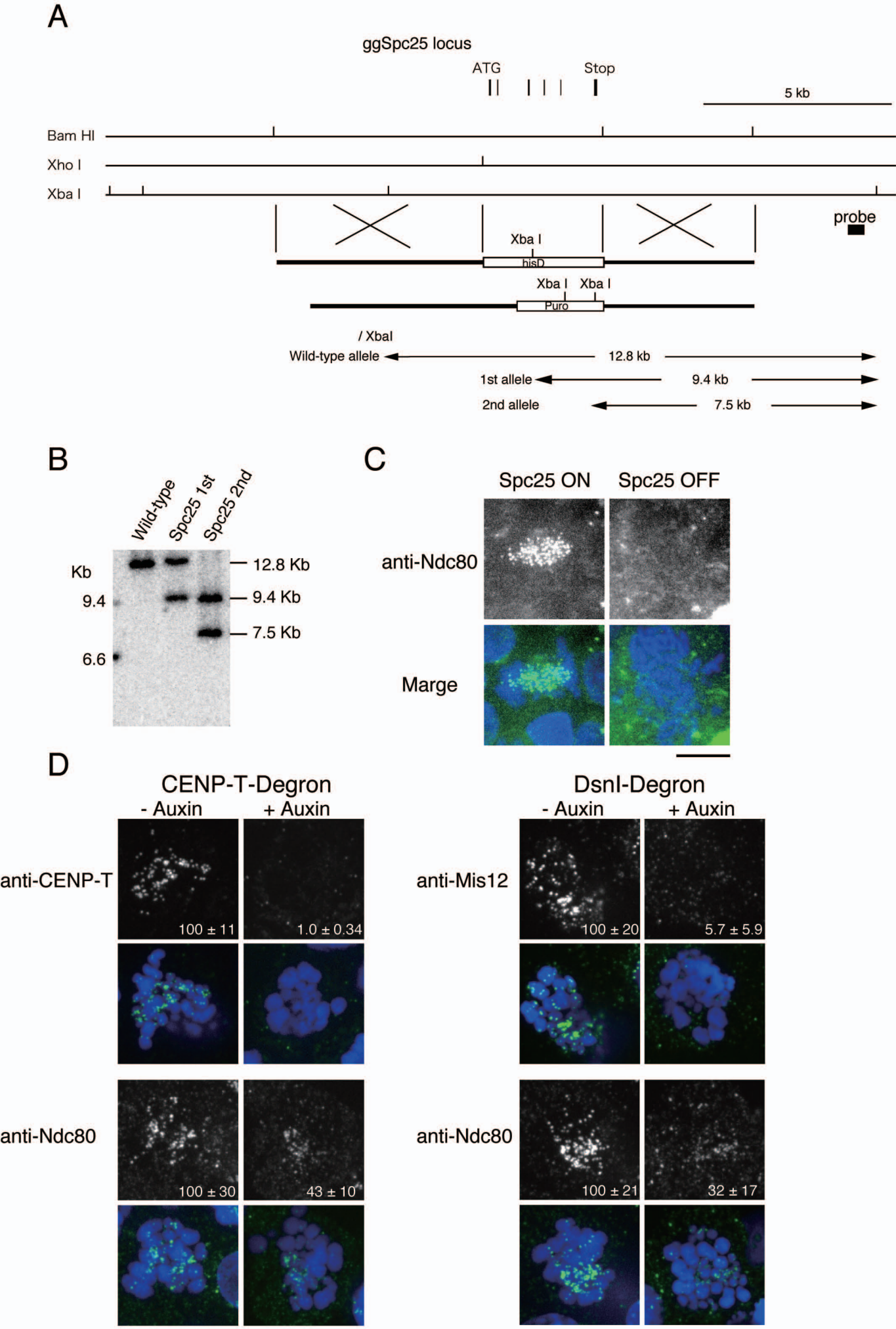

Nishino et al., 2012 Figure S6